

# Higher-order flow coefficients in dilepton emission from a magnetized hadronic medium

Rajkumar Mondal<sup>✉\*</sup> and Defu Hou<sup>†</sup>

<sup>a</sup>*Institute of Particle Physics and Key Laboratory of Quark and Lepton Physics (MOS),  
Central China Normal University, Wuhan 430079, China*

The study of dilepton emission from hot hadronic matter provides a unique probe of the medium properties in heavy-ion collisions. In the presence of strong magnetic fields expected in non-central collisions, the emission spectrum can develop anisotropic features. While the impact of a magnetic field on the dilepton emission rate has been explored, the detailed higher-order azimuthal anisotropy—characterized by flow coefficients beyond elliptic flow—remains an open question, particularly in the low invariant-mass region where medium effects are most pronounced. We investigate higher-order anisotropy in the dilepton emission rate from a magnetized hot hadronic medium. Our results reveal a continuous dilepton spectrum with strong Landau-cut contributions at low invariant masses due to the background magnetic field. The emission rate exhibits significant azimuthal-angle dependence in this region, characterized by flow coefficients  $v_n$ . Odd coefficients vanish by symmetry, while the elliptic flow  $v_2$  is positive and oscillatory at low invariant masses—driven by Landau-level quantization of pions—but negligible at higher masses. Higher-order coefficients  $v_4, v_6$  show similar trends, with notable structures at low masses and negligible values at higher masses. The transverse-momentum dependence increases with magnetic field strength, while temperature effects are minimal. Our findings demonstrate that the magnetic field induces significant higher-order azimuthal anisotropy in dilepton emission at low invariant masses, with  $v_2, v_4, v_6$  exhibiting distinct oscillatory behavior linked to pion Landau quantization. This resolves the gap in understanding the anisotropic response of dilepton emission in magnetized media. The results highlight dileptons as sensitive probes of magnetic-field effects in heavy-ion collisions, offering new avenues to constrain field strengths and hadronic dynamics in the quark-gluon plasma.

## I. Introduction

Strongly interacting hot and dense nuclear matter, composed of quarks or hadrons, is anticipated to be created at relativistic heavy-ion collisions (HICs) experiments at facilities like the Relativistic Heavy Ion Collider (RHIC) at Brookhaven National Laboratory and the Large Hadron Collider (LHC) at CERN. Such matter may also exist in the cores of compact astrophysical objects, such as neutron stars. The collision of two nuclei at ultra-relativistic energies leads to the liberation of the fundamental constituents of the nucleons forming a deconfined state of quarks and gluons, is known as the quark-gluon plasma (QGP) in local thermal equilibrium [1–4]. The matter created in HICs undergoes rapid cooling due to expansion driven by its own pressure gradient, undergoing various stages of evolution. However, direct observation of this process is strongly hindered due to its transient ( $\sim$  few fm/c) nature of the process. Consequently, researchers must rely on indirect probes and observables such as spectra of electromagnetic probes (photon and dileptons), heavy quark production, quarkonia suppression, jet energy loss, collective flow,  $J/\Psi$  suppression etc to extract microscopic as well as bulk properties of the create matter. Among these, electromagnetic probes (photons and dileptons), owing to their large mean free paths, are the most effective one for characterizing the space-time history of the collision [5–12]. In the QGP, quarks and antiquarks can annihilate to form a virtual photon, which subsequently decays into a dilepton pair. The dilepton emission rate from this process has been widely studied in Refs. [6, 9, 10]. In heavy-ion collisions, however, several other thermal and non-thermal sources also produce dileptons and create a sizable background [1, 10, 11, 13]. Among these, the Drell–Yan process is one of the most important and is well understood within perturbative QCD [1, 11, 14–16]. Dileptons are also produced from the decays of hadronic resonances such as  $\pi^0$ ,  $\rho$ ,  $\omega$ , and  $J/\psi$ , and their yields can be estimated experimentally through invariant-mass analysis [1]. However, separating the photons and dileptons originating from the hadronic medium, formed after the phase transition or crossover, is challenging. Therefore, a reliable theoretical estimate of the photon and dilepton yields from a hot and dense hadronic medium, including the possible modification of hadronic properties below the critical temperature, is crucial for identifying electromagnetic signals from the QGP. Extensive studies have shown that the dilepton emission rate from the hadronic phase is significantly modified in the low invariant mass region [5, 8, 17–19].

It is well accepted that a very strong magnetic field is produced in non-central or asymmetric HICs experiments at the Relativistic Heavy Ion Collider or Large Hadron Collider, in the cores of neutron stars, and during the early universe. The estimated value of the magnetic field in the HIC experiment is around  $10^{15-18}$  Gauss [20–23] generated by the rapid movement of electrically charged spectators in the early stages of the collision. Although it experiences rapid decay within a few fm/c, the finite electrical conductivity ( $\sim$  a few MeV) of the medium can possibly delay the decay process sufficiently allowing a

\* [rajkumarmondal.phy@gmail.com](mailto:rajkumarmondal.phy@gmail.com) / [rajkumarmondal.phy@zohomail.in](mailto:rajkumarmondal.phy@zohomail.in)

† [houdf@ccnu.edu.cn](mailto:houdf@ccnu.edu.cn)

nonzero magnetic field to persist even during the subsequent hadronic phase following the phase transition or crossover from the Quark-Gluon Plasma (QGP) [24–26]. The magnitude of the magnetic field in astrophysical objects such as the interior of neutron stars, magnetars is of the order of  $10^{15}$  Gauss. The strength of these magnetic fields is comparable to the typical energy scale of quantum chromodynamics (QCD), affecting various microscopic and macroscopic properties of strongly interacting matter (Refs. [27–29] for reviews). These fields lead to various exotic phenomena [29] in strongly interacting matter due to the complex vacuum structure of QCD such as Chiral Magnetic Effect (CME), Chiral Vortical Effect (CVE), Magnetic Catalysis (MC), and Inverse Magnetic Catalysis (IMC) etc. The effects of magnetic field on the transport properties from hadronic medium have been studied in Refs. [26, 30–35]. Estimation of shear and bulk viscosity has been made in different approaches from magnetically modified hadronic matter in Refs. [30–33]. The effects of magnetic field on the electrical conductivity from a strongly interacting hadron gas has been studied in Refs. [26, 34].

The presence of magnetic field significantly modifies the emission of electromagnetic probes. Dilepton production from the QGP medium under such conditions has been extensively explored in the literature by many authors [36–47] employing various approximations. For instance, Ref. [48], investigates the ellipticity of photon emission from a hot magnetized QCD plasma, while Ref. [46] determines the ellipticity parameter ( $v_2$ ) for dileptons emission from a magnetized quark-gluon-plasma showing that  $v_2$  tends to be positive and large at large transverse momenta. Higher-order anisotropy coefficients in photon and dilepton emission from QGP are discussed in Ref. [49]. As the system expands and cools from the QGP state, hadronic matter forms and serves as a significant source of dilepton production, particularly in the low invariant mass region. Recent studies in Refs. [50, 51] analyze dilepton production and its elliptic flow parameter ( $v_2$ ) from a magnetized hadronic medium in terms of the spectral function of  $\rho^0$  which is evaluated from the electromagnetic vector current correlation function using the real time formalism of thermal field theory. In the present article, we extend these efforts to investigate the higher-order angular dependence of dilepton emission rates from a magnetized hadronic medium. To the best of our knowledge, such a study has not yet been performed.

The article is organized as follows: Section II presents the general formalism for anisotropy in the dilepton production rate, expressed in terms of the spectral function in a thermomagnetic background. Section III discusses the numerical results, and Section IV provides a summary and conclusions.

## II. Formalism

### A. Dilepton emission rate from hadronic medium

In a hadronic medium, dileptons are generated through hadronic resonances, where a virtual photon emitted during a hadronic transition subsequently decays into a lepton–antilepton pair. The method for evaluating dilepton production from a hot hadronic medium is well established in earlier studies [6, 7, 12, 19, 52, 53]. But, for the sake of completeness, we only summarize the main steps required for our analysis following the approach of Ref. [19].

We consider a transition from an initial thermal state  $|i\rangle = |I(\mathcal{P}_I)\rangle$  with momentum  $\mathcal{P}_I$  goes towards a final state  $|f\rangle = |H(\mathcal{P}_H); l(p), \bar{l}(p')\rangle$  consisting of hadrons with momentum  $\mathcal{P}_H$  plus emitted dilepton carries four-momentum  $q^\mu = p^\mu + p'^\mu$ . Such transition probability is determined from the squared matrix element  $|\langle f|\hat{S}|i\rangle|^2$  where the scattering matrix operator is expressed as

$$\hat{S} = \tau_c \exp\left[i \int d^4x \mathcal{L}_{\text{int}}(x)\right], \quad (1)$$

in which  $\tau_c$  denotes the time-ordering operator and the interaction Lagrangian density relevant for the electromagnetic processes is

$$\mathcal{L}_{\text{int}} = -e \left[ J_\mu^l(x) + J_\mu^h(x) \right] \mathcal{A}^\mu(x). \quad (2)$$

$J_\mu^l(x) = e\bar{\psi}(x)\gamma_\mu\psi(x)$  and  $J_\mu^h(x)$  are representing the conserved leptonic and hadronic electromagnetic currents respectively and are coupled by the photon field represented by  $\mathcal{A}^\mu(x)$ . The leading nonvanishing contribution to the transition amplitude arises at second order in the interaction. Expanding the scattering operator  $\hat{S}$  to this order, only the mixed hadronic–leptonic term contributes to the matrix element  $\langle f|\hat{S}|i\rangle$ . The resulting contribution can be written as

$$\langle f|\hat{S}|i\rangle = - \int d^4x_1 d^4x_2 \langle H|J_\mu^h(x_1)|I\rangle \langle l, \bar{l}|J_\nu^l(x_2)|0\rangle \Delta_F^{\mu\nu}(x_1 - x_2) \quad (3)$$

where  $\Delta_F^{\mu\nu}(x_1 - x_2)$  denotes photon propagator. The associated Feynman diagram is shown in Fig. 1. Disconnected Feynman diagram do not contribute to the process and are therefore omitted. After straightforward calculations, the squared matrix element

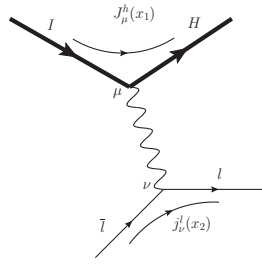


Figure 1. Feynman diagram for dilepton production from hadronic medium.

per unit four-volume becomes

$$|\langle f | \hat{S} | i \rangle|^2 = (2\pi)^2 \delta^{(4)}(\mathcal{P}_I - \mathcal{P}_H - q) \frac{e^4}{q^4} l^{\mu\nu} \langle H | J_\mu^h(0) | I \rangle \langle I | J_\nu^h(0) | H \rangle, \quad (4)$$

where the leptonic tensor is given by

$$l^{\mu\nu} = 4[p^\mu p'^\nu + p^\nu p'^\mu - (p \cdot p' + m_l^2)g^{\mu\nu}] \quad (5)$$

with  $m_l$  as leptonic mass. Assuming local thermal equilibrium, leads to

$$\sum_{I,H} Z^{-1} e^{-\beta \mathcal{P}_I^0} |\langle f | \hat{S} | i \rangle|^2 = \frac{e^4}{q^4} e^{-\beta q_0} l^{\mu\nu} \int d^4x e^{iq \cdot x} \langle J_\mu^h(x) J_\nu^h(0) \rangle \quad (6)$$

where  $\beta = \frac{1}{T}$  is inverse temperature and  $Z$  the partition function of the system. The dilepton multiplicity from thermal hadronic medium is then obtained by summing over the final states and averaging over the initial states, given by the relation:

$$N = \sum_{\text{spin}} \sum_{I,H} Z^{-1} e^{-\beta \mathcal{P}_I^0} |\langle f | \hat{S} | i \rangle|^2. \quad (7)$$

Introducing  $\int d^4q \delta^{(4)}(q - p - p') = 1$  and performing the phase-space integrations, the dilepton emission rate per unit four-volume can be written as

$$\frac{dN}{d^4x} = \int d^4q L^{\mu\nu} \int d^4x e^{iq \cdot x} \langle J_\mu^h(x) J_\nu^h(0) \rangle, \quad (8)$$

where

$$L^{\mu\nu} = \frac{1}{(2\pi)^6} \frac{2\pi}{3} \left( 1 + \frac{2m_l^2}{q^2} \right) \sqrt{1 - \frac{4m_l^2}{q^2}} (q^\mu q^\nu - q^2 g^{\mu\nu}). \quad (9)$$

The differential dilepton emission per unit space-time four-volume follows as

$$\frac{dN}{d^4x d^4q} = \frac{\alpha^2}{6\pi^3 q^2} e^{-\beta q_0} L(q^2) [-g_{\mu\nu} M^{+\mu\nu}(q)], \quad (10)$$

with  $\alpha$  as the fine-structure constant, the leptonic contributions is

$$L(q^2) = \sqrt{1 - \frac{4m_l^2}{q^2}} \left( 1 + \frac{2m_l^2}{q^2} \right) \quad (11)$$

and Fourier transform of two-point vector current correlator is

$$M^{+\mu\nu}(q) = \int d^4x e^{iq \cdot x} \langle J_\mu^h(x) J_\nu^h(0) \rangle. \quad (12)$$

In the real-time formalism of thermal field theory, the correlator assumes a  $2 \times 2$  matrix structure on account of the shape of contour in complex time plane. Fourier transform of the time-ordered two-point is

$$M_{ab}^{\mu\nu} = i \int d^4x e^{iq \cdot x} \langle T_c [J_h^\mu(x) J_h^\nu(0)] \rangle_{ab} \quad (13)$$

where  $T_c$  is time-ordering operator for the contour  $c$  and the thermal indices  $a, b \in \{1, 2\}$  indicate that the two points can be chosen on either of the two horizontal segments of the time contour  $c$ . It can be diagonalized as

$$M^{\mu\nu} = U \begin{pmatrix} \bar{M}^{\mu\nu} & 0 \\ 0 & -\bar{M}^{*\mu\nu} \end{pmatrix} U, \quad (14)$$

with  $U = \begin{pmatrix} \sqrt{n+1} & \sqrt{n} \\ \sqrt{n} & \sqrt{n+1} \end{pmatrix}$  containing the thermal distribution function  $n = (e^{\beta|q_0|} - 1)^{-1}$ . The diagonal element  $\bar{M}^{\mu\nu}$  in Eq. (14) is an analytic function and it is related to the 11 component via

$$\text{Re } \bar{M}^{\mu\nu}(q) = \text{Re } M_{11}^{\mu\nu}(q), \quad (15)$$

$$\text{Im } \bar{M}^{\mu\nu}(q) = \tanh\left(\frac{|q_0|}{2T}\right) \text{Im } M_{11}^{\mu\nu}(q). \quad (16)$$

Using the spectral representation, one finds

$$M^{+\mu\nu}(q) = \frac{2e^{\beta q_0}}{e^{\beta q_0} - 1} \text{Im } \bar{M}^{\mu\nu}(q) = \epsilon(q^0) \frac{2e^{\beta q_0}}{e^{\beta q_0} + 1} \text{Im } M^{\mu\nu}(q) \quad (17)$$

where  $\epsilon(q^0)$  is sign function. Substitution Eq. (17) into Eq. (10), we obtain the dilepton production rate (DPR) as

$$\frac{dN}{d^4x d^4q} = \frac{\alpha^2}{3\pi^3 q^2} \frac{1}{e^{\beta q_0} - 1} L(q^2) [-g_{\mu\nu} \text{Im } \bar{M}^{\mu\nu}(q)]. \quad (18)$$

To compute the DPR, we require an explicit form of the local hadronic current. Within the Vector Meson Dominance (VMD) framework, considering isovector  $\rho$ -meson, the conserved hadronic current can be expressed as

$$J_h^\mu(x) = J_\rho^\mu(x) = F_\rho m_\rho \rho^\mu(x), \quad (19)$$

where  $\rho^\mu(x)$  denotes the Heisenberg field corresponding to the  $\rho^0$ -meson, the coupling  $F_\rho = 156$  MeV is fixed from the decay rate  $\Gamma_{\rho^0 \rightarrow e^+e^-} = 7.0$  keV. Therefore, the dilepton production rate then becomes

$$\frac{dN}{d^4x d^4q} = \frac{\alpha^2}{\pi^3 q^2} f_{\text{BE}}(q_0) L(q^2) F_\rho^2 m_\rho^2 \mathcal{A}(q; T), \quad (20)$$

where  $f_{\text{BE}}(x) = (e^{x/T} - 1)^{-1}$  represents the Bose-Einstein thermal distribution function and the in-medium  $\rho^0$  spectral function is

$$\mathcal{A}(q; T) = -\frac{1}{3} g^{\mu\nu} \text{Im } \bar{D}_{\mu\nu}(q)$$

with  $\bar{D}_{\mu\nu}(q)$  as a full  $\rho_0$ -meson propagator. In a thermo-magnetic background, the  $\rho_0$  spectral function will be modified and given by the relation

$$\mathcal{A}(q; T, eB) = -\frac{1}{3} g^{\mu\nu} \text{Im } D_{\mu\nu}(q)$$

and it is presented later in Sec. II C.

## B. Flow coefficients for dilepton emission in a background magnetic field

The flow coefficients provide a powerful way to understand the geometry, evaluation, electromagnetic structure of the emitting medium. We follow the geometry shown in Fig. 2 to study the anisotropy of the dilepton emission rate in the presence of a background magnetic field. For simplicity, we take the magnetic field to be constant and oriented along the  $z$ -axis, while the beam direction is chosen along the  $x$ -axis. With this setup, the transverse momentum of the dilepton lies in the  $y$ - $z$  plane, which is perpendicular to the beam direction. The azimuthal angle  $\phi$  is defined with respect to the reaction plane, i.e., the  $x$ - $y$  plane shown in Fig. 2. In non-central heavy-ion collisions, the differential dilepton emission rate is typically expressed as a Fourier

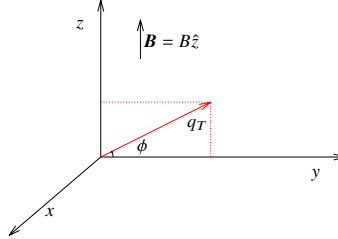


Figure 2. A schematic diagram of the coordinate frame used in this work

expansion in the azimuthal angle relative to the reaction plane, expressed by [54],

$$\frac{dN}{d^4x d^4q} = \frac{1}{2\pi} \frac{dN}{d^4x M dM q_T dq_T dy} \left[ 1 + \sum_{n=1}^{\infty} 2v_n \cos \{n(\phi - \phi_{re})\} \right] \quad (21)$$

where  $\phi_{re}$  denotes the reaction-plane angle. The dilepton four-momentum is written as

$$q^\mu = (q^0, \mathbf{q}) \equiv (q^0, q_x, q_y, q_z) \equiv (q^0, q_x, q_T \cos \phi, q_T \sin \phi)$$

with  $q_T = \sqrt{q_y^2 + q_z^2}$  being the transverse momentum. The infinitesimal four-momentum element is

$$d^4q = M dM q_T dq_T d\phi dy$$

where  $M = \sqrt{q^2}$  is the invariant mass and the rapidity describing motion of the particle is

$$y = \frac{1}{2} \ln \left( \frac{q_0 + q_x}{q_0 - q_x} \right).$$

Dilepton production from the hadronic medium peaks transverse to the beam direction because the medium is densest at mid-rapidity, while the rapid longitudinal expansion suppresses emission along the beam axis. In this setup,  $q_x = 0$  corresponds to mid-rapidity or central rapidity. The flow coefficients  $v_n$  are obtained as the Fourier coefficients of the azimuthal dependence of the dilepton emission rate:

$$v_n = \frac{\int_0^{2\pi} \frac{dN}{d^4x d^4q} \cos(n\phi) d\phi}{\int_0^{2\pi} \frac{dN}{d^4x d^4q} d\phi}. \quad (22)$$

The denominator in Eq. (22) represents the total differential dilepton emission rate. The formalism for dilepton emission from a thermal hadronic medium has been studied in the previous Sec. II A.

## C. Rho-meson spectral function in a background magnetic field

The key quantity in the dilepton emission rate from hadronic matter is the in-medium spectral function of the  $\rho^0$ , which is evaluated using the Vector Meson Dominance (VMD) model in the presence of a background magnetic field [17–19]. This spectral function corresponds to the imaginary part of the full  $\rho^0$  propagator and contains the dynamics of the hadronic medium. It can be obtained by solving the Dyson-Schwinger equation, which relates the  $\rho^0$  self-energy  $\Pi^{\mu\nu}$  and the bare propagator

$D_0^{\mu\nu}$  [19, 55]:

$$D^{\mu\nu} = D_0^{\mu\nu} - D_0^{\mu\beta} \Pi_{\beta\alpha} D^{\alpha\nu} \quad (23)$$

where the bare propagator is

$$D_0^{\mu\nu}(q) = \frac{-1}{q^2 - m_\rho^2 + i\epsilon} \left( -g^{\mu\nu} + \frac{q^\mu q^\nu}{m_\rho^2} \right).$$

We perform a Lorentz decomposition of the  $\rho^0$  self-energy in the presence of a magnetic field to obtain the spectral function  $\mathcal{A}(q; T, eB)$  [50]:

$$\Pi^{\mu\nu}(T, eB) = \Pi_1 \mathcal{P}_1^{\mu\nu} + \Pi_2 \mathcal{P}_2^{\mu\nu} + \Pi_3 \mathcal{P}_3^{\mu\nu} + \Pi_4 \mathcal{P}_4^{\mu\nu}. \quad (24)$$

Here,  $\mathcal{P}_1^{\mu\nu}$ ,  $\mathcal{P}_2^{\mu\nu}$ ,  $\mathcal{P}_3^{\mu\nu}$ , and  $\mathcal{P}_4^{\mu\nu}$  are basis tensors and the corresponding form factors  $\Pi_1$ ,  $\Pi_2$ ,  $\Pi_3$  and  $\Pi_4$  are given by

$$\begin{aligned} \mathcal{P}_1^{\mu\nu} &= \frac{\tilde{u}^\mu \tilde{u}^\nu}{\tilde{u}^2}, & \mathcal{P}_2^{\mu\nu} &= g^{\mu\nu} - \frac{q^\mu q^\nu}{q^2} - \frac{\tilde{u}^\mu \tilde{u}^\nu}{\tilde{u}^2} - \frac{\tilde{b}^\mu \tilde{b}^\nu}{\tilde{b}^2}, \\ \mathcal{P}_3^{\mu\nu} &= \frac{\tilde{b}^\mu \tilde{b}^\nu}{\tilde{b}^2}, & \mathcal{P}_4^{\mu\nu} &= \frac{1}{\sqrt{\tilde{u}^2 \tilde{b}^2}} (\tilde{u}^\mu \tilde{b}^\nu + \tilde{u}^\nu \tilde{b}^\mu), \end{aligned} \quad (25)$$

$$\begin{aligned} \Pi_1 &= \frac{1}{\tilde{u}^2} u_\mu u_\nu \Pi^{\mu\nu}, & \Pi_2 &= g_{\mu\nu} \Pi^{\mu\nu} - \Pi_1 - \Pi_3, \\ \Pi_3 &= \frac{1}{\tilde{b}^2} \left[ b_\mu b_\nu \Pi^{\mu\nu} + \frac{(b \cdot \tilde{u})^2}{\tilde{u}^2} \Pi_1 - 2 \frac{b \cdot \tilde{u}}{\tilde{u}^2} u_\mu b_\nu \Pi^{\mu\nu} \right], \end{aligned} \quad (26)$$

$$\Pi_4 = \frac{1}{\sqrt{\tilde{u}^2 \tilde{b}^2}} (u_\mu b_\nu \Pi^{\mu\nu} - (b \cdot \tilde{u}) \Pi_1). \quad (27)$$

In Eqs. (25)–(27), the vectors are defined as

$$\tilde{u}^\mu = u^\mu - \frac{q \cdot u}{q^2} q^\mu, \quad \tilde{b}^\mu = b^\mu - \frac{q \cdot b}{q^2} q^\mu - \frac{b \cdot \tilde{u}}{\tilde{u}^2} \tilde{u}^\mu,$$

where  $u^\mu$  is the medium four-velocity and

$$b^\mu = \frac{1}{2B} \varepsilon^{\mu\nu\alpha\beta} F_{\nu\alpha}^{\text{ex}} u_\beta,$$

with  $F_{\nu\alpha}^{\text{ex}}$  being the electromagnetic field strength tensor representing the external magnetic field. In the local rest frame (LRF), these reduce to

$$u_{\text{LRF}}^\mu = (1, \mathbf{0}), \quad b_{\text{LRF}}^\mu = (0, \hat{z}),$$

where  $\hat{z}$  is along the direction of the external magnetic field. Using the Lorentz decomposition, the full  $\rho^0$  propagator in a magnetic background is then expressed as

$$\begin{aligned} D^{\mu\nu}(T, eB) &= \frac{\mathcal{P}_2^{\mu\nu}}{q^2 - m_\rho^2 + \Pi_2} + \frac{(q^2 - m_\rho^2 + \Pi_1) \mathcal{P}_3^{\mu\nu}}{(q^2 - m_\rho^2 + \Pi_3)(q^2 - m_\rho^2 + \Pi_1) - \Pi_4^2} - \frac{\Pi_4 \mathcal{P}_4^{\mu\nu}}{(q^2 - m_\rho^2 + \Pi_1)(q^2 - m_\rho^2 + \Pi_3) - \Pi_4^2} \\ &+ \frac{(q^2 - m_\rho^2 + \Pi_3) \mathcal{P}_1^{\mu\nu}}{(q^2 - m_\rho^2 + \Pi_3)(q^2 - m_\rho^2 + \Pi_1) - \Pi_4^2} - \frac{q^\mu q^\nu}{q^2 m_\rho^2}. \end{aligned} \quad (28)$$

The imaginary part of Eq. (28) is used to obtain the spectral function  $\mathcal{A}(q; T, eB)$ , which is then employed to calculate the dilepton production rate. The analytic form of the  $\rho^0$  self-energy is obtained using an effective field theory of hadrons, where

the  $\rho$ -meson interacts with pions via the interaction Lagrangian density [56]:

$$\mathcal{L}_{\text{int}} = -g_{\rho\pi\pi} (\partial_\mu \rho_\nu) \cdot (\partial^\mu \pi \times \partial^\nu \pi), \quad (29)$$

where  $\rho_\nu$  and  $\pi$  are the isovector fields representing the  $\rho$ -mesons and pions respectively. The coupling constant  $g_{\rho\pi\pi} = 20.72 \text{ GeV}^{-2}$  is fixed from the decay width  $\Gamma_{\rho \rightarrow \pi\pi} = 155.8 \text{ MeV}$ . The corresponding Feynman diagram for the one-loop self-energy of  $\rho^0$  is shown in Fig. 3. To calculate the thermomagnetic  $\rho^0$  self-energy, we employ the real-time formalism (RTF) of finite-temperature field theory. In RTF, the self-energy, which is a two-point function, forms a  $2 \times 2$  matrix, but only the 11-component is needed for the calculations of analytic self-energy [19]. It can be expressed as  $\text{Im } \Pi^{\mu\nu}(q) = \tanh\left(\frac{|q^0|}{2T}\right) \text{Im } \Pi_{11}^{\mu\nu}(q)$  and  $\text{Re } \Pi^{\mu\nu}(q) = \text{Re } \Pi_{11}^{\mu\nu}(q)$ . Using the interaction Lagrangian in Eq. (29), the 11-component of the  $\rho^0$  one-loop self-energy is obtained as [50, 57]:

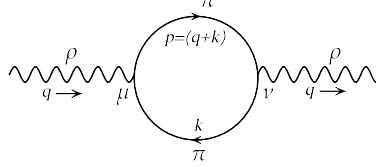


Figure 3. Feynman diagram for the one-loop self-energy of the  $\rho^0$  meson[50].

$$\Pi_{11}^{\mu\nu}(q; T, eB) = i \int \frac{d^4 k}{(2\pi)^4} \mathcal{N}^{\mu\nu}(q, k) D_{11}^{\text{MagF}}(k) D_{11}^{\text{MagF}}(p = q + k), \quad (30)$$

where  $\mathcal{N}^{\mu\nu}(q, k)$  contains the vertex factors and is given by:

$$\mathcal{N}^{\mu\nu}(q, k) = g_{\rho\pi\pi}^2 \left[ k^\mu k^\nu q^4 + q^\mu q^\nu (q \cdot k)^2 - (q^\mu k^\nu + q^\nu k^\mu) (q \cdot k) q^2 \right]. \quad (31)$$

Here,  $D_{11}^{\text{MagF}}(p)$  is the 11-component of the charged pion propagator, given by the expression [57, 58]:

$$D_{11}^{\text{MagF}}(p) = \sum_{l=0}^{\infty} 2(-1)^l L_l(2\alpha_p) e^{-\alpha_p} \left[ 2\pi i \eta(p \cdot u) \delta(p_\parallel^2 - m_l^2) + \frac{-1}{p_\parallel^2 - m_l^2 + i\epsilon} \right], \quad (32)$$

where the sum runs over Landau levels  $l$ ,  $\alpha_p = -p_\perp^2/eB$ , and  $m_l = \sqrt{m_\pi^2 + eB(2l+1)}$  is the effective pion mass.  $L_l(z)$  denotes the Laguerre polynomial of order  $l$ , and  $\eta(x) = \Theta(x) f_{\text{BE}}(x) + \Theta(-x) f_{\text{BE}}(-x)$ , with  $\Theta(x)$  being the Heaviside step function. The components of the momentum are defined as  $p_{\parallel,\perp}^\mu = g_{\parallel,\perp}^{\mu\nu} p_\nu$  with  $g_{\parallel}^{\mu\nu} = \text{diag}(1, 0, 0, -1)$  and  $g_{\perp}^{\mu\nu} = \text{diag}(0, -1, -1, 0)$ . In this convention,  $p_\parallel^2 = p_0^2 - p_z^2$  and  $p_\perp^2 = -(p_x^2 + p_y^2)$ . Now, substituting Eq. (32) into Eq. (30) and performing the  $dk^0$  integration, we obtain the real and imaginary parts of the  $\rho^0$  self-energy as

$$\begin{aligned} \text{Re } \Pi^{\mu\nu}(q; T, eB) &= \text{Re } \Pi_{\text{vac}}^{\mu\nu}(q, eB) + \sum_{n=0}^{\infty} \sum_{l=0}^{\infty} \int_{-\infty}^{\infty} \frac{dk_z}{2\pi} \mathcal{P} \left[ \frac{f_l^k}{2\omega_l^k} \left\{ \frac{N_{nl}^{\mu\nu}(q, k^0 = -\omega_l^k, k_z)}{(q^0 - \omega_l^k)^2 - (\omega_n^p)^2} + \frac{N_{nl}^{\mu\nu}(q, k^0 = \omega_l^k, k_z)}{(q^0 + \omega_l^k)^2 - (\omega_n^p)^2} \right\} \right. \\ &\quad \left. + \frac{f_n^p}{2\omega_n^p} \left\{ \frac{N_{nl}^{\mu\nu}(q, k^0 = -q^0 - \omega_n^p, k_z)}{(q^0 + \omega_n^p)^2 - (\omega_l^k)^2} + \frac{N_{nl}^{\mu\nu}(q, k^0 = -q^0 + \omega_n^p, k_z)}{(q^0 - \omega_n^p)^2 - (\omega_l^k)^2} \right\} \right], \quad (33) \end{aligned}$$

$$\begin{aligned} \text{Im } \Pi^{\mu\nu}(q; T, eB) &= -\tanh\left(\frac{|q^0|}{2T}\right) \pi \sum_{n=0}^{\infty} \sum_{l=0}^{\infty} \int_{-\infty}^{\infty} \frac{dk_z}{2\pi} \frac{1}{4\omega_l^k \omega_n^p} \\ &\quad \times \left[ (1 + f_l^k + f_n^p + 2f_l^k f_n^p) \left\{ N_{nl}^{\mu\nu}(q, k^0 = -\omega_l^k, k_z) \delta(q^0 - \omega_l^k - \omega_n^p) \right. \right. \\ &\quad \left. \left. + N_{nl}^{\mu\nu}(q, k^0 = \omega_l^k, k_z) \delta(q^0 + \omega_l^k + \omega_n^p) \right\} \right. \\ &\quad \left. + (f_l^k + f_n^p + 2f_l^k f_n^p) \left\{ N_{nl}^{\mu\nu}(q, k^0 = -\omega_l^k, k_z) \delta(q^0 - \omega_l^k + \omega_n^p) \right. \right. \end{aligned}$$

$$+N_{nl}^{\mu\nu}(q, k^0 = \omega_l^k, k_z) \delta(q^0 + \omega_l^k - \omega_n^p) \Big]. \quad (34)$$

where

$$\omega_l^k = \sqrt{k_z^2 + m_l^2}, \quad \omega_n^p = \sqrt{p_z^2 + m_n^2}, \quad f_l^k = f_{\text{BE}}(\omega_l^k), \quad f_n^p = f_{\text{BE}}(\omega_n^p),$$

and

$$\tilde{N}_{nl}^{\mu\nu}(q, k_\perp, k_\parallel) = 4(-1)^{n+l} e^{-\alpha_k - \alpha_p} N^{\mu\nu} L_l(2\alpha_k) L_n(2\alpha_p), \quad N_{nl}^{\mu\nu}(q, k_\parallel) = \int \frac{d^2 k_\perp}{(2\pi)^2} \tilde{N}_{nl}^{\mu\nu}(q, k_\perp, k_\parallel).$$

Further, the imaginary part of self-energy can be simplified doing  $dk_z$  integration, obtained as

$$\begin{aligned} \text{Im } \Pi^{\mu\nu}(q; T, eB) = & -\tanh\left(\frac{|q^0|}{2T}\right) \sum_{n=0}^{\infty} \sum_{l=0}^{\infty} \frac{1}{4\lambda^{1/2}(q_\parallel^2, m_l^2, m_n^2)} \sum_{k_z \in \{k_z^\pm\}} \left[ (1 + f_l^k + f_n^p + 2f_l^k f_n^p) \right. \\ & \times \left\{ \Theta\left(q^0 - \sqrt{q_z^2 + (m_l + m_n)^2}\right) N_{nl}^{\mu\nu}(q, k^0 = -\omega_l^k, k_z) \right. \\ & + \Theta\left(-q^0 - \sqrt{q_z^2 + (m_l + m_n)^2}\right) N_{nl}^{\mu\nu}(q, k^0 = \omega_l^k, k_z) \Big\} \\ & + (f_l^k + f_n^p + 2f_l^k f_n^p) \left\{ \Theta\left(q^0 - \min(q_z, E^\pm)\right) \Theta\left(-q^0 + \max(q_z, E^\pm)\right) N_{nl}^{\mu\nu}(q, k^0 = -\omega_l^k, k_z) \right. \\ & \left. \left. + \Theta\left(-q^0 - \min(q_z, E^\pm)\right) \Theta\left(q^0 + \max(q_z, E^\pm)\right) N_{nl}^{\mu\nu}(q, k^0 = \omega_l^k, k_z) \right\} \right]. \quad (35) \end{aligned}$$

Here,  $\lambda(x, y, z) = x^2 + y^2 + z^2 - 2xy - 2yz - 2zx$  is the Källén function,

$$k_z^\pm = \frac{-\tilde{q}_\parallel^2 q_z \pm |q^0| \lambda^{1/2}(q_\parallel^2, m_l^2, m_n^2)}{2q_\parallel^2}, \quad \tilde{q}_\parallel^2 = q_\parallel^2 + m_l^2 - m_n^2, \quad E^\pm = \frac{m_l - m_n}{|m_l \pm m_n|} \sqrt{q_z^2 + (m_l \pm m_n)^2}.$$

In Eq. (35), the  $\Theta$ -functions represent branch cuts in the complex energy plane of the  $\rho^0$  and correspond to kinematically allowed scattering and decay processes involving charged pions in different Landau levels. Due to dimensional reduction in a magnetic field, these cuts involve only the longitudinal dynamics. Unlike the  $eB = 0$  case, a nontrivial Landau-cut contribution can appear in the physical timelike region even when the loop particles have identical masses. This occurs when the pions in the loop occupy different Landau levels. Physically, this means that a  $\rho$  meson can be absorbed through the scattering of a pion in a lower Landau level, producing a pion in a higher Landau level (and the reverse process). The Unitary-I and Unitary-II contributions are nonvanishing in the kinematic regions

$$\sqrt{q_z^2 + 4(m_\pi^2 + eB)} < q^0 < \infty,$$

and

$$-\infty < q^0 < -\sqrt{q_z^2 + 4(m_\pi^2 + eB)},$$

respectively. On the other hand, the nonvanishing kinematic domain for the Landau cuts is

$$|q^0| < \max(q_z, E_\pm).$$

Detailed discussions can be found in Refs. [50, 57] and has not repeated here.

### III. Numerical Results

In this section, we present numerical results for the dilepton production rate and its azimuthal angle dependence as function of invariant mass  $M$ , transverse momentum  $q_T$  with respect to beam axis (see Fig. 2) for central rapidity ( $q_x = 0$ ) from a

magnetized hadronic matter. It should be noted that while calculating DPR and its azimuthal angle dependence, we have to perform a sum over infinite number of Landau levels. However, for all numerical results, we have taken up to 500 Landau levels which ensures the convergence of the sum. Since we are interested for hadronic stage of the matter created in HICs, we have chosen two representative values of temperature,  $T = 130$  and  $160$  MeV respectively. As the hadrons are created in the later stages of the evaluation processes in HICs, it is expected that the strength of background field should be smaller compared to the QGP phase. Hence, we have chosen the lowest value of magnetic field  $eB = 0.01$  GeV<sup>2</sup> and a higher value of magnetic field  $eB = 0.05$  GeV<sup>2</sup> to understand the interplay between magnetic field and thermal effects. Since the magnetic field is oriented along the  $z$ -axis, it breaks rotational symmetry in the plane perpendicular to the beam direction. Consequently, the dilepton production rate (DPR) is expected to exhibit azimuthal-angle dependence, i.e., anisotropy in the transverse plane relative to the beam. To investigate this, we analyze various flow coefficients of dilepton emission at mid-rapidity (central rapidity) under different physical conditions. The numerical evaluation of the integral in denominator of Eq. (22) can be simplified employing spatial symmetries of the magnetized matter at mid rapidity [46]. Firstly, we note that, with our choice of axes, the system is invariant under spatial rotation about  $z$  axis, which is a subgroup of the spatial rotation group that remains unbroken in  $B \neq 0$  case. Invoking this symmetry we can write

$$\frac{dN}{d^4x d^4q}(\pi - \phi) = \frac{dN}{d^4x d^4q}(\phi).$$

Again, since the magnetic field is an axial vector, there is also a reflection symmetry with respect to the reaction plane. This will allow us to write

$$\frac{dN}{d^4x d^4q}(\phi) = \frac{dN}{d^4x d^4q}(-\phi).$$

Hence, we need to evaluate the integral only in the first quadrant, i.e.  $0 \leq \phi < \pi/2$ . The results for the other three quadrants can be evaluated using the above symmetries.

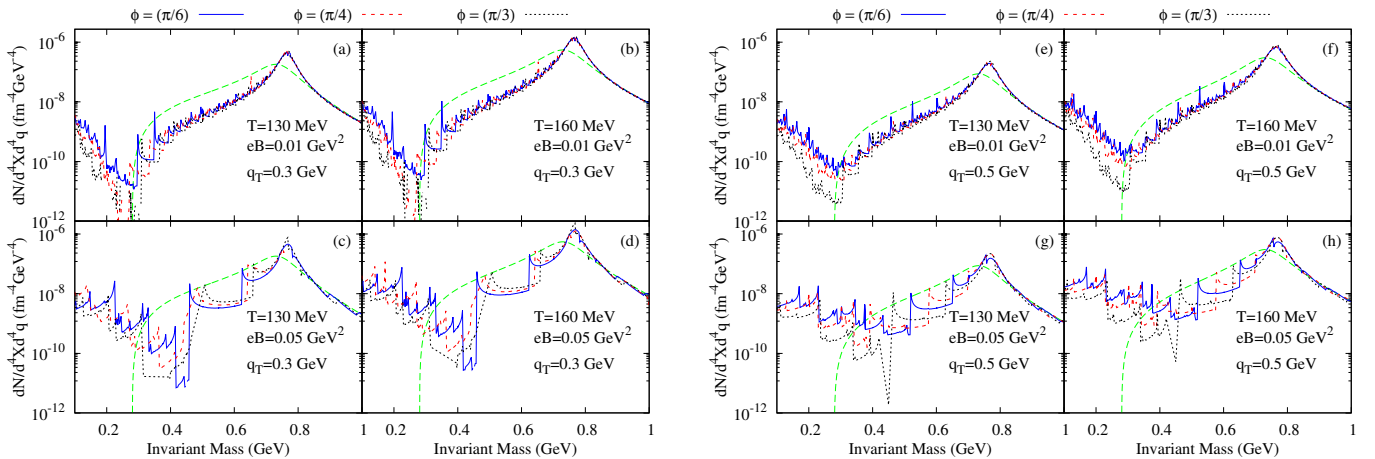


Figure 4. (Color online) The dilepton production rate as a function of invariant mass for  $eB = 0.01, 0.05$  GeV<sup>2</sup> and  $T = 130, 160$  MeV at azimuthal angle  $\phi = \frac{\pi}{6}, \frac{\pi}{4}, \frac{\pi}{3}$  in (a)-(d) for  $q_T = 0.3$  GeV and (e)-(h) for  $q_T = 0.5$  GeV. Green color line corresponds Born Rate ( $eB = 0$ ).

Figs. 4(a)-(d) for  $q = 0.3$  GeV and Figs. 4(e)-(h) for  $q = 0.5$  GeV show the variation of the dilepton production rate as a function invariant mass for different values of azimuthal angle  $\phi$ , magnetic field  $eB$  and temperature  $T$ . For comparison, the born rate in absence of the background field (green dashed line) have also shown which is consistent with the earlier observations by C. Gale and J. Kapusta in Refs. [7, 17]. Figs. 4(a)-(d) as well as Figs. 4(e)-(h) contain a set of four panels in which  $T$  increases in the horizontal direction and  $eB$  increases in the downward direction. To begin the discussion, we focus on Figs. 4(a)-(d). It is evident from the plots that the dilepton emission rate is highly enhanced in the low invariant mass region compared to the born rate (in absence of  $eB$ ) owing to the Landau cut contributions. This is a purely magnetic field dependent effect and can be connected to the process where  $\rho$ -meson is absorbed by means of scattering with a pion in lower Landau level and producing a pion in higher Landau level in the final state (and the time reversed process) because pion mass is modified by the external magnetic field, given by the expression  $m_l = \sqrt{m_\pi^2 + eB(2l + 1)}$  (see below of Eq. (32)). The last two terms of Eq. (35) include Landau cut contributions. The DPR in higher invariant mass region is dominated by the unitary cut contributions corresponding to the decay process  $\rho_0 \rightarrow \pi^+\pi^-$ . These can be connected to the first two terms of Eq. (35). A detailed study regarding of these different cuts structure of kinematic domain can be found in Ref. [50, 57]. Moreover, because the lepton masses are

negligible compared to the pion mass, the threshold invariant mass for dilepton production aligns with the  $\rho$ -meson mass for all magnetic-field strengths and temperatures. Furthermore, an increase in temperature leads to a noticeable rise in the overall magnitude of the DPR as evident from the comparison between Figs. 4(a) and 4(b). This behavior stems from the enhanced thermal phase space at higher temperatures. It is worth to mention that when  $q_T$  is along the  $z$ -direction, the Landau and Unitary cut contributions are separated, creating a forbidden gap that is independent of temperature and the background magnetic field [50]. This arises because a pion in Landau level  $n$  can interact with pions in levels  $n - 1$ ,  $n$ , or  $n + 1$  to produce a  $\rho$ -meson. In contrast, in our study,  $q_T$  points in a different or arbitrary direction, resulting in a continuous dilepton emission spectrum. To study the azimuthal angle dependence of DPR, we have chosen representative values of  $\phi = \frac{\pi}{3}$ ,  $\frac{\pi}{4}$ ,  $\frac{\pi}{6}$  as the knowledge of dilepton emission in first quadrant is sufficient to evaluate the results in the other three quadrants. It is clear from the figures that dilepton production rate has a non-trivial azimuthal angle dependence in the low invariant mass region. As the magnetic strength increases, the  $\phi$ -dependence qualitatively increases as comparing between Figs. 4(a) and (c). On the other hand, the rate has negligible  $\phi$  dependence for higher values of invariant mass of dilepton indicating an isotropic emission of high mass dileptons. The spikes in the DPR arises due to the “threshold singularities” which appear whenever the energy of the virtual photon becomes equal to one of the numerous Landau-level thresholds. This can also be explained mathematically using Eq. (35), where the Källén function in the denominator vanishes at each threshold of the cut, as defined by the unit step function. However, this nonsmooth nature of DPR spectrums do not lead to any generic trend in azimuthal angle dependence. Finally, for a given value of  $eB$  and  $T$ , the overall DPR is suppressed with larger value of  $q_T$  which is evident by comparing Fig. 4(a) and Fig. 4(e). It is connected with the modification of effective temperature of the medium. Therefore, observed thermal suppression is primarily due to the Bose-Einstein distribution appearing in the DPR expression in Eq. (20). Further reduction can be attributed to the spectral function or equivalently the imaginary part of the  $\rho^0$  self-energy (see Appendix), which also involves Bose-Einstein distribution function. However, obtaining a quantitative estimate requires a complete space-time evolution of this rate within magneto-hydrodynamics, which lies beyond the scope of the present study. In addition, the magnitude of emission rate increases with the increasing temperature due to increase of the thermal phase space.

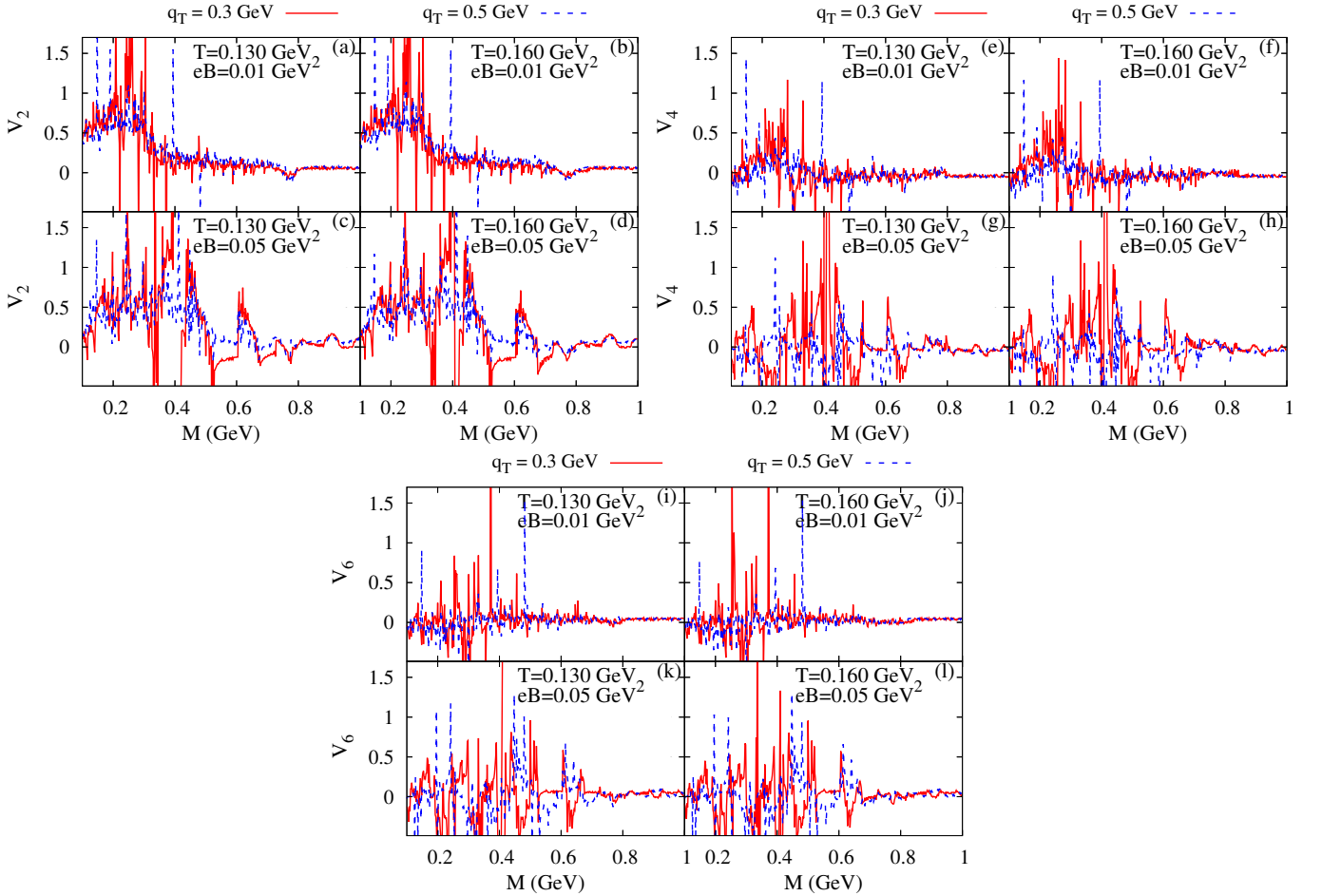


Figure 5. (Color online) The flow coefficient ( $v_n$ ) in (a)-(d) for  $v_2$ , (e)-(h) for  $v_4$  and (i)-(l) for  $v_6$  as a function of invariant mass ( $M$ ) for  $eB = 0.01, 0.05 \text{ GeV}^2$  and  $q_T = 0.3, 0.5 \text{ GeV}$  at  $T = 130 \text{ MeV}$  and  $T = 160 \text{ MeV}$ .

As discussed earlier, the anisotropy in dilepton production can be quantified by analyzing flow coefficients ( $v_n$ ) defined in Eq. (22). The odd flow coefficients (particularly  $v_1, v_3$ ) vanish because the dilepton emission rate is symmetric under the transformation  $\phi \rightarrow \pi - \phi$  as discussed in the beginning of this section. Hence, we only analyze the even flow coefficients for dilepton emission in this section. Figs. 5(a)-(d) show variation of the ellipticity parameter ( $v_2$ ) as a function of invariant mass for different transverse momenta in the similar setting namely in the horizontal (downward) direction the temperature (background magnetic field) increases keeping  $eB(T)$  constant. The numerical data reveal various qualitative features, which are also influenced by the emergence of several spike-like structures associated with numerous Landau level quantization and numerous threshold effects. The figure shows that  $v_2$  has a strong tendency to remain positive in low invariant mass region. A positive value of  $v_2$  reflects an oblate shape of the DPR indicating that dilepton production is more pronounced in the direction transverse to the background field, i.e.  $\phi \sim 0$  which aligns with the reaction plane. Furthermore,  $v_2$  displays oscillations increasing with the increase of magnetic field at low invariant mass region and the oscillations become negligible at high invariant mass region suggesting that the DPR becomes nearly isotropic, a trend also evident in the earlier figures Figs. 4(a)-(h). The figure (for example Fig. 5(a)) also indicates a general upward trend of  $v_2$  with increasing  $q_T$ . The  $q_T$  dependence on  $v_2$  is more evident with the large value of magnetic field as observed from Figs. 5(a) and (c) or Figs. 5(b) and (d). The qualitative behavior of  $v_2$  seen in Figs. 5(a)-(d) consistent with earlier results reported in Ref. [46] on dilepton emission from a magnetized quark-gluon plasma. Now, we extend our analysis to higher-order anisotropy coefficients  $v_4$  and  $v_6$ . It probe finer details of the medium in heavy-ion collisions. We will concentrate our attention on the same kinematic region. The numerical results for dilepton  $v_4$  are shown in Figs. 5(e)-(h). As before, the four panels show results under identical conditions: temperature (or magnetic field) increases horizontally (or downward) with constant  $eB(T)$ . It is observed that the coefficient  $v_4$  tends to be positive at low invariant masses, indicating significant anisotropy in the DPR. However, the value of  $v_4$  becomes negligible at higher invariant masses. Here, also  $q_T$  dependence of  $v_4$  is prominent with increasing magnetic field. The results for dilepton  $v_6$  are presented in Figs. 5(i)-(l) with four panels, temperature (or magnetic field) increases horizontally (or downward) with constant  $eB(T)$ . The dilepton  $v_6$  fluctuates at low invariant mass but remains nearly zero at higher invariant masses. Similar to  $v_2$  and  $v_4$ , the  $q_T$  dependence on  $v_6$  significantly increased with increasing magnetic field. Notably, we observe well-pronounced modulations in the  $v_n$  dependence on the invariant mass. In addition to the alternating sign pattern, the high-resolution data exhibit other intriguing features. A comparison of the results in Figs. 5(a)–(l) reveals correlated peak patterns across all anisotropy coefficients, particularly in the low invariant mass region. Such features arise due to the Landau-level quantization of pions. The oscillation in the flow coefficients  $v_n$  arises from the so called threshold singularities, decreases with the increasing magnetic field. In addition, the coefficients does not show any strong dependence on temperature.

#### IV. Summary & Conclusion

Our study demonstrates that a background magnetic field significantly modifies the dilepton production rate (DPR) and its azimuthal anisotropy in a hot hadronic medium. The key findings — enhanced DPR at low invariant masses due to the Landau cut, strong azimuthal anisotropy quantified by oscillatory flow coefficients ( $v_2, v_4, v_6$ ) in the same mass region, and isotropic emission at higher invariant masses — provide a clear picture of magnetically induced effects in a static medium.

These results can be contextualized within the broader literature on electromagnetic probes in heavy-ion collisions. The enhancement of the DPR at low invariant masses aligns with prior theoretical works highlighting the role of the Landau cut in the presence of magnetic fields [57, 59]. Our calculation, which explicitly incorporates the thermomagnetic spectral function of the  $\rho^0$  meson via the Dyson–Schwinger equation, offers a concrete microscopic mechanism for this enhancement: the scattering of  $\rho^0$  mesons with charged pions occupying quantized Landau levels. This is a purely magnetic phenomenon, absent in a zero-field scenario. The negligible magnetic effect we observe in the high invariant mass region, dominated by the unitary cut, is consistent with the understanding that the two-pion continuum threshold is less sensitive to moderate external fields. The most significant implication of our work lies in the quantification of intrinsic anisotropy. The positive and oscillatory  $v_2$ , along with non-zero higher-order coefficients ( $v_4, v_6$ ), at low invariant masses establish that a static, magnetized medium itself is an anisotropic source of dilepton emission. This finding is crucial because it suggests that the azimuthal anisotropy coefficients ( $v_n$ ) measured in heavy-ion collisions likely receive contributions from two distinct sources: (i) the collective hydrodynamic flow of the medium, and (ii) the intrinsic anisotropy induced by the strong, early-stage magnetic field. Our analysis, conducted in the rest frame of the medium, isolates and elucidates the latter contribution.

However, several limitations of this study must be acknowledged. First, our model assumes a constant, uniform magnetic field in a static, infinite medium. In an actual heavy-ion collision, the magnetic field is extremely transient, decaying rapidly with time, and is highly inhomogeneous. Second, we have not considered the concurrent evolution of the medium — its expansion, cooling, and the gradual dilution of the magnetic field. These dynamic aspects are critical for direct phenomenological comparison with experimental data. Third, the hadronic medium is treated in a simplified manner; potential effects from other hadronic states or a phase transition to a quark-gluon plasma are not included.

Given these limitations, the logical direction for future research is clear. To bridge the gap between our static, magnetized calculation and the dynamic reality of heavy-ion collisions, detailed numerical simulations are essential. Future work should

employ phenomenological frameworks, such as relativistic hydrodynamic or transport simulations, that self-consistently incorporate both the spacetime evolution of the hot medium and that of the embedded electromagnetic fields. Such simulations could convolve the intrinsic anisotropic emission rates calculated here with a realistic fireball evolution to produce predictions for the final observed  $v_n$  coefficients. This would allow for a quantitative separation of hydrodynamic and magnetic contributions to dilepton anisotropy.

In conclusion, our findings provide strong qualitative evidence that a background magnetic field acts as an intrinsic source of azimuthal anisotropy in dilepton emission. While definitive claims regarding the use of this anisotropy as a clean signature of primordial magnetic fields in experiments require the aforementioned sophisticated, integrated simulations, this work establishes a foundational mechanism and provides benchmark results for such future endeavors.

## V. ACKNOWLEDGMENT

Authors thank Prof. Sourav Sarkar, Prof. Pradip Roy, Dr. Nilanjan Chaudhuri, and Dr. Snigdha Ghosh for valuable discussions at various stages of this work. Rajkumar Mondal is supported by Central China Normal University and by research grant from Prof. Defu Hou. Defu Hou's research is supported in part by the National Key Research and Development Program of China under Contract No. 2022YFA1604900. Additionally, Defu Hou receives partial support from the National Natural Science Foundation of China (NSFC) under Grant No.12435009, and No. 12275104.

- 
- [1] C. Y. Wong, *Introduction to high-energy heavy ion collisions* (1995).
  - [2] S. Sarkar, H. Satz, and B. Sinha, eds., *The physics of the quark-gluon plasma*, Vol. 785 (2010).
  - [3] W. Florkowski, *Phenomenology of Ultra-Relativistic Heavy-Ion Collisions* (2010).
  - [4] H. Satz, *Extreme states of matter in strong interaction physics. An introduction*, Vol. 841 (Springer Verlag, New York, 2012).
  - [5] L. D. McLerran and T. Toimela, *Phys. Rev. D* **31**, 545 (1985).
  - [6] K. Kajantie, J. I. Kapusta, L. D. McLerran, and A. Mekjian, *Phys. Rev. D* **34**, 2746 (1986).
  - [7] C. Gale and J. I. Kapusta, *Phys. Rev. C* **38**, 2659 (1988).
  - [8] H. A. Weldon, *Phys. Rev. D* **42**, 2384 (1990).
  - [9] P. V. Ruuskanen, *Nucl. Phys. A* **525**, 255 (1991).
  - [10] P. V. Ruuskanen, *Nucl. Phys. A* **544**, 169 (1992).
  - [11] J. Alam, B. Sinha, and S. Raha, *Phys. Rept.* **273**, 243 (1996).
  - [12] J. Alam, S. Sarkar, P. Roy, T. Hatsuda, and B. Sinha, *Annals Phys.* **286**, 159 (2001), [arXiv:hep-ph/9909267](#).
  - [13] W. Cassing and E. L. Bratkovskaya, *Phys. Rept.* **308**, 65 (1999).
  - [14] N. S. Craigie, *Phys. Rept.* **47**, 1 (1978).
  - [15] C. Grosso-Pilcher and M. J. Shochet, *Ann. Rev. Nucl. Part. Sci.* **36**, 1 (1986).
  - [16] R. Brock *et al.* (CTEQ), *Rev. Mod. Phys.* **67**, 157 (1995).
  - [17] C. Gale and J. I. Kapusta, *Nucl. Phys. B* **357**, 65 (1991).
  - [18] R. Rapp and J. Wambach, *Adv. Nucl. Phys.* **25**, 1 (2000), [arXiv:hep-ph/9909229](#).
  - [19] S. Mallik and S. Sarkar, *Hadrons at Finite Temperature* (Cambridge University Press, Cambridge, 2016).
  - [20] K. Tuchin, *Adv. High Energy Phys.* **2013**, 490495 (2013), [arXiv:1301.0099 \[hep-ph\]](#).
  - [21] D. E. Kharzeev, L. D. McLerran, and H. J. Warringa, *Nucl. Phys. A* **803**, 227 (2008), [arXiv:0711.0950 \[hep-ph\]](#).
  - [22] V. Skokov, A. Y. Illarionov, and V. Toneev, *Int. J. Mod. Phys. A* **24**, 5925 (2009), [arXiv:0907.1396 \[nucl-th\]](#).
  - [23] K. Tuchin, *Phys. Rev. C* **88**, 024911 (2013), [arXiv:1305.5806 \[hep-ph\]](#).
  - [24] U. Gursoy, D. Kharzeev, and K. Rajagopal, *Phys. Rev. C* **89**, 054905 (2014), [arXiv:1401.3805 \[hep-ph\]](#).
  - [25] G. Inghirami, L. Del Zanna, A. Beraudo, M. H. Moggaddam, F. Becattini, and M. Bleicher, *Eur. Phys. J. C* **76**, 659 (2016), [arXiv:1609.03042 \[hep-ph\]](#).
  - [26] P. Kalikotay, S. Ghosh, N. Chaudhuri, P. Roy, and S. Sarkar, *Phys. Rev. D* **102**, 076007 (2020), [arXiv:2009.10493 \[hep-ph\]](#).
  - [27] B. Friman, C. Hohne, J. Knoll, S. Leupold, J. Randrup, R. Rapp, and P. Senger, eds., *The CBM physics book: Compressed baryonic matter in laboratory experiments*, Vol. 814 (2011).
  - [28] V. A. Miransky and I. A. Shovkovy, *Phys. Rept.* **576**, 1 (2015), [arXiv:1503.00732 \[hep-ph\]](#).
  - [29] D. Kharzeev, K. Landsteiner, A. Schmitt, and H.-U. Yee, eds., *Strongly Interacting Matter in Magnetic Fields*, Vol. 871 (2013).
  - [30] G. Kadam, *Mod. Phys. Lett. A* **30**, 1550031 (2015), [arXiv:1412.5303 \[hep-ph\]](#).
  - [31] A. Das, H. Mishra, and R. K. Mohapatra, *Phys. Rev. D* **100**, 114004 (2019), [arXiv:1909.06202 \[hep-ph\]](#).
  - [32] A. Dash, S. Samanta, J. Dey, U. Gangopadhyaya, S. Ghosh, and V. Roy, *Phys. Rev. D* **102**, 016016 (2020), [arXiv:2002.08781 \[nucl-th\]](#).
  - [33] R. Ghosh and N. Haque, *Phys. Rev. D* **105**, 114029 (2022), [arXiv:2204.01639 \[hep-ph\]](#).
  - [34] A. Das, H. Mishra, and R. K. Mohapatra, *Phys. Rev. D* **99**, 094031 (2019), [arXiv:1903.03938 \[hep-ph\]](#).
  - [35] A. Das, H. Mishra, and R. K. Mohapatra, *Phys. Rev. D* **102**, 014030 (2020), [arXiv:2004.04665 \[hep-ph\]](#).
  - [36] K. Tuchin, *Phys. Rev. C* **87**, 024912 (2013), [arXiv:1206.0485 \[hep-ph\]](#).
  - [37] K. Tuchin, *Phys. Rev. C* **88**, 024910 (2013), [arXiv:1305.0545 \[nucl-th\]](#).
  - [38] N. Sadooghi and F. Taghinavaz, *Annals Phys.* **376**, 218 (2017), [arXiv:1601.04887 \[hep-ph\]](#).

- [39] A. Bandyopadhyay, C. A. Islam, and M. G. Mustafa, *Phys. Rev. D* **94**, 114034 (2016), arXiv:1602.06769 [hep-ph].
- [40] A. Bandyopadhyay and S. Mallik, *Phys. Rev. D* **95**, 074019 (2017), arXiv:1704.01364 [hep-ph].
- [41] S. Ghosh and V. Chandra, *Phys. Rev. D* **98**, 076006 (2018), arXiv:1808.05176 [hep-ph].
- [42] C. A. Islam, A. Bandyopadhyay, P. K. Roy, and S. Sarkar, *Phys. Rev. D* **99**, 094028 (2019), arXiv:1812.10380 [hep-ph].
- [43] S. Ghosh, N. Chaudhuri, S. Sarkar, and P. Roy, *Phys. Rev. D* **101**, 096002 (2020), arXiv:2004.09203 [nucl-th].
- [44] K. Hattori, H. Taya, and S. Yoshida, *JHEP* **01**, 093 (2021), arXiv:2010.13492 [hep-ph].
- [45] N. Chaudhuri, S. Ghosh, S. Sarkar, and P. Roy, *Phys. Rev. D* **103**, 096021 (2021), arXiv:2104.11425 [hep-ph].
- [46] X. Wang and I. A. Shovkovy, *Phys. Rev. D* **106**, 036014 (2022), arXiv:2205.00276 [nucl-th].
- [47] A. Das, A. Bandyopadhyay, and C. A. Islam, *Phys. Rev. D* **106**, 056021 (2022), arXiv:2109.00019 [hep-ph].
- [48] X. Wang, I. A. Shovkovy, L. Yu, and M. Huang, *Phys. Rev. D* **102**, 076010 (2020), arXiv:2006.16254 [hep-ph].
- [49] X. Wang and I. A. Shovkovy, *Phys. Rev. D* **109**, 056008 (2024), arXiv:2307.07557 [hep-ph].
- [50] R. Mondal, N. Chaudhuri, S. Ghosh, S. Sarkar, and P. Roy, *Phys. Rev. D* **107**, 036017 (2023), arXiv:2301.09475 [hep-ph].
- [51] R. Mondal, N. Chaudhuri, S. Ghosh, S. Sarkar, and P. Roy, *Eur. Phys. J. A* **59**, 287 (2023), arXiv:2311.17632 [hep-ph].
- [52] C. Gale and J. I. Kapusta, *Phys. Rev. C* **35**, 2107 (1987).
- [53] P. V. Ruuskanen, *Adv. Ser. Direct. High Energy Phys.* **6**, 519 (1990).
- [54] S. Voloshin and Y. Zhang, *Z. Phys. C* **70**, 665 (1996), arXiv:hep-ph/9407282.
- [55] M. L. Bellac, *Thermal Field Theory*, Cambridge Monographs on Mathematical Physics (Cambridge University Press, 2011).
- [56] O. Krehl, C. Hanhart, S. Krewald, and J. Speth, *Phys. Rev. C* **62**, 025207 (2000), arXiv:nucl-th/9911080.
- [57] S. Ghosh, A. Mukherjee, P. Roy, and S. Sarkar, *Phys. Rev. D* **99**, 096004 (2019), arXiv:1901.02290 [hep-ph].
- [58] A. Ayala, P. Mercado, and C. Villavicencio, *Phys. Rev. C* **95**, 014904 (2017), arXiv:1609.02595 [hep-ph].
- [59] K. Hattori and K. Itakura, *Annals Phys.* **330**, 23 (2013), arXiv:1209.2663 [hep-ph].